Available online at www.sciencedirect.com

ScienceDirect

Ceramics International 40 (2014) 2373–2379

CERAMICS INTERNATIONAL

www.elsevier.com/locate/ceramint

Phase stability and microstructure of manganese-doped calcia-stabilized zirconia heat treated in a reducing atmosphere

Yen-Lin Huang[a], Ying-Chieh Lee[b], Du-Cheng Tsai[a], Rong-Hsin Huang[a], Fuh-Sheng Shieu[a,*]

[a]Department of Materials Science and Engineering, National Chung Hsing University, 250 Kuo Kuang Road, Taichung 40227, Taiwan
[b]Department of Materials Engineering, National PingTung University of Science & Technology, 1 Shuefu Road, Neipu, Pingtung 91201, Taiwan

Received 21 May 2013; received in revised form 31 July 2013; accepted 1 August 2013
Available online 9 August 2013

Abstract

The effects of Mn_3O_4 addition and annealing under a reducing atmosphere (N_2:H_2=97:3) on the microstructure and phase stability of calcia-stabilized zirconia (CSZ) ceramics sintered at 1500 °C for 3 h in air were investigated. Undoped and Mn_3O_4-doped 12.5 mol% CSZ (125CSZ) ceramics were prepared via a conventional solid-state reaction process. X-ray diffraction patterns showed a single cubic phase of ZrO_2 in 0.3 mol % Mn_3O_4-doped 125CSZ after sintering at 1500 °C for 3 h. Monoclinic ZrO_2 phases were observed in 0.5 mol% Mn_3O_4-doped 125CSZ and undoped 15 mol% CSZ ceramic after annealing at 1300 °C for 30 cycles in a reducing atmosphere. The amount of monoclinic ZrO_2 phase observed in 0.5 mol% Mn_3O_4-doped 125CSZ was less than that found in undoped 15 mol% CSZ annealed at 1300 °C under a reducing atmosphere.

Keywords: Aging test; Calcia stabilized zirconia (CSZ); Manganese; Oxygen partial pressures

1. Introduction

Calcia-stabilized zirconia (CSZ) has received considerable attention from the research community because of its excellent features, which include high oxygen-ion conductivity, high fracture toughness, and low thermal conductivity. CSZ is widely applied in solid oxide fuel cells, thermal barrier coatings, and advanced structural ceramics [1–6]. Pure zirconia (ZrO_2) has a cubic fluorite structure upon cooling from its melting point (2680 °C) and transforms into a tetragonal form at 2370 °C and a monoclinic form at 1170 °C [7]. The metastable cubic phase of ZrO_2 is the most suitable for application in many devices, and one of the major challenges of working with the material is controlling and tuning its crystallographic phase. Introduction of cations with less than four valence electrons, such as Y^{3+}, Ca^{2+}, and Mg^{2+}, creates a high concentration of oxygen vacancies that can stabilize high-temperature structure phases at room temperature. According to a two-component phase diagram (ZrO_2–CaO) [8,9], ZrO_2 can be stabilized in a cubic fluorite structure at low temperatures with calcium oxide (CaO) contents between 10 and 20 mol% at 1700 °C.

Manganese ions can dissolve into yttria-stabilized ZrO_2 (YSZ) with a solubility limit of 5 mol% at 1000 °C and 15 mol% at 1500 °C [10]. Appel et al. [11] reported that a single cubic structure could be retained by 7.5 mol% YSZ with 2 mol% or more Mn at 1400 °C. The valence state of Mn may change with the oxygen partial pressure [12]. Kawada et al. [10] found that all Mn^{3+} in stabilized ZrO_2 could be reduced to Mn^{2+} at oxygen partial pressures lower than 10^{-10} Pa. Therefore, oxygen vacancies are generated when Mn^{2+} ions are substituted into the Zr^{4+} site at low oxygen partial pressures. Moreover, oxygen vacancies have been reported to exert very important effects that can retain the high symmetry of the crystal phase of ZrO_2 at room temperature [13].

To date, no information is yet available regarding the synthesis and phase stability of Mn-doped CSZ, which is crucial for device applications. In the current study, the phase stability and microstructure of CSZ ceramics doped with 0–0.5 mol% Mn_3O_4 were investigated. The effect of annealing under a reducing atmosphere on the phase stability of Mn-doped CSZ ceramics was thoroughly studied by X-ray diffraction (XRD) and scanning electron microscopy (SEM).

*Corresponding author. Tel.: +88 642 284 0500; fax: +88 642 285 7017.
E-mail address: fsshieu@dragon.nchu.edu.tw (F.-S. Shieu).

0272-8842/$ - see front matter © 2013 Elsevier Ltd and Techna Group S.r.l. All rights reserved.
http://dx.doi.org/10.1016/j.ceramint.2013.08.008

2. Materials and methods

A conventional solid-state reaction method was used to prepare 3, 6, 7.5, 10, 12.5, and 15 mol% CaO-stabilized ZrO_2 from commercial powders of ZrO_2 (KCM Corporation, Japan, $>99.9\%$) and CaO (Strem Chemicals Inc., USA, $>99.9\%$). The ZrO_2 and CaO powders were mixed with deionized water and ZrO_2 balls having 2 mm diameter in a ball-milling bottle for 24 h (ball-to-water-to-powder ratio, 12:2:1; rotation rate, 62 rpm). The mixture was dried at 125 °C, calcined at 1400 °C for 6 h in air, and then crushed into powder. The powders were mixed with the binder (polyvinyl alcohol) additive and then pressed into disk-shaped specimens. The pellets were sintered at 1300, 1400, or 1500 °C for 3 h in air at a heating rate of 3 °C/min. Different amounts of Mn_3O_4 (0.1, 0.2, 0.3, or 0.5 mol%) were mixed with 12.5 mol% CaO-stabilized ZrO_2 (125CSZ) powders using the same procedure, and the pellets were sintered at 1500 °C for 3 h in air at a heating rate of 3 °C/min.

The undoped 15 mol% CSZ (15CSZ) and 0.5 mol% Mn_3O_4-doped 125CSZ (Mn125CSZ) ceramics were subjected to thermal aging tests. The samples were annealed at 1300 °C for 2 h at a heating rate of 5 °C/min in flowing dry gas (N_2:H_2 = 97:3) and subsequently cooled in a tube furnace; one annealing and cooling procedure is considered one cycle in the thermal aging test. The oxygen partial pressure of the dry gas mix was about 1×10^{-10} Pa.

The crystallinity of the sintered samples were analyzed by high-resolution XRD (Bruker D8D, Germany), with Cu-$K\alpha$ radiation for 2θ from 20 ° to 80 ° at a scan speed of 2 °/min^{-1}. The DIFFRAC plus TOPAS version 3.0 program was used to determine the phase fractions of the constituent phases of the CSZ samples. Interior microstructural observation of the sintered ceramics was conducted using SEM (JEOL JEL-6400, Tokyo, Japan). Average grain size measurements were conducted using a linear intercept method in compliance with the British Standard BS EN 623-3:2001, where the number of grains analyzed per sample was about 400. The bulk density of the sintered pellets was measured using the Archimedes method; 10 samples were used to obtain average values.

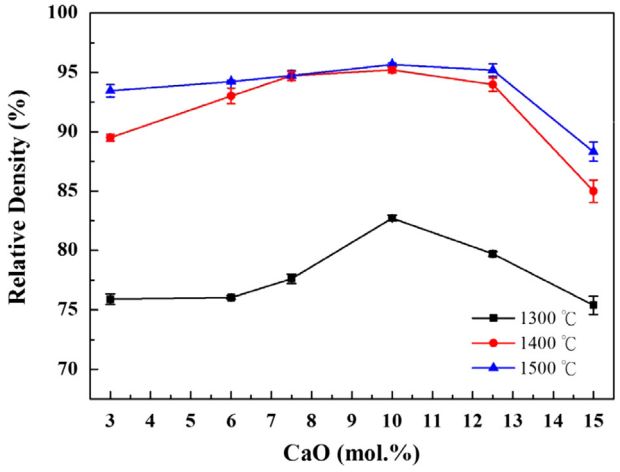

Fig. 1. Relative density as a function of CaO addition for ZrO_2 ceramics sintered at 1300, 1400, and 1500 °C for 3 h.

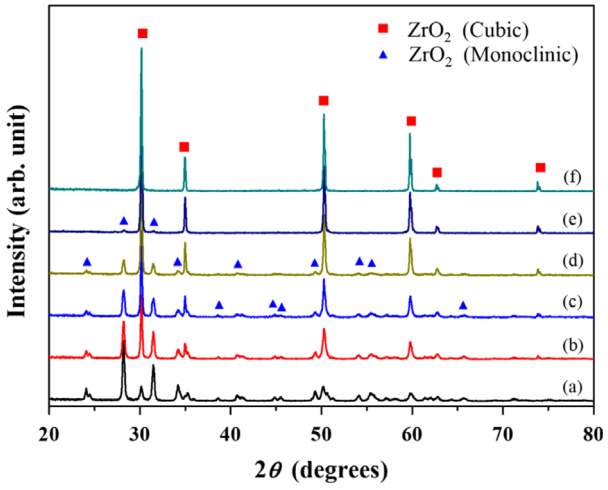

Fig. 2. XRD spectra of the ZrO_2 ceramics with (a) 3, (b) 6, (c) 7.5, (d) 10, (e) 12.5, (f) 15 mol% CaO addition sintered at 1500 °C for 3 h.

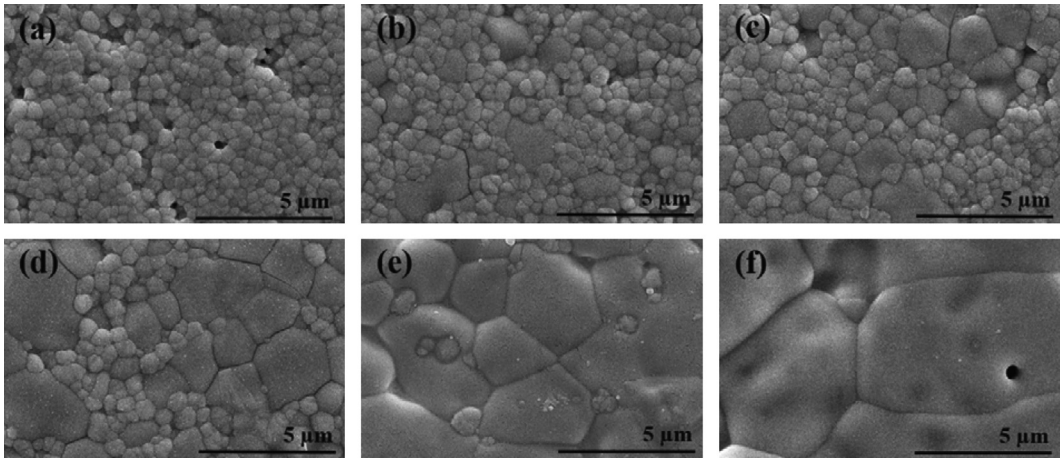

Fig. 3. SEM micrographs of the ZrO_2 ceramics with (a) 3, (b) 6, (c) 7.5, (d) 10, (e) 12.5, (f) 15 mol% CaO addition sintered at 1500 °C for 3 h.

3. Results and discussion

3.1. Synthesis of CSZ and Mn_3O_4-doped CSZ

The relative densities of the ZrO_2 ceramics sintered at different temperatures (1300, 1400, and 1500 °C) for 3 h were determined as a function of CaO addition and are plotted in Fig. 1. The relative densities of the specimens sintered at all temperatures increased with increasing CaO content up to 10 mol%. Ceramics with a relatively high density of 95.7% were obtained. Radford et al. [14] reported that enhancement of densification may be observed in 5 wt% CSZ ceramics with 5 mol% CaO. However, the relative density decreased with increasing CaO addition at CaO contents over 10 mol%. The relative density of 15 mol% CaO-added ZrO_2 ceramic decreased to 88.3%. The decrease in density can be attributed to the increase in CaO concentration in the samples, which causes an increase in number of generated oxygen vacancies because of the different valence states of Ca^{2+} and Zr^{4+} [15].

The crystalline phases of the CSZ samples were determined by XRD. Fig. 2 shows the XRD spectra of ZrO_2 ceramics with 3, 6, 7.5, 10, 12.5, and 15 mol% CaO and sintered at 1500 °C for 3 h. ZrO_2 ceramic has cubic and monoclinic phases (c-ZrO_2 and m-ZrO_2) when the CaO content is less than 12.5 mol%. The intensity of the peaks of monoclinic phases decreased significantly as the CaO content increased to 12.5 mol% and then disappeared when the CaO content reached 15 mol%.

Fig. 3 presents SEM micrographs showing different surface morphologies of the ZrO_2 ceramics with 3, 6, 7.5, 10, 12.5, and 15 mol% CaO and sintered at 1500 °C for 3 h. The number of small grains decreased with increasing CaO content [Fig. 3(a)-(e)]. According to the XRD analysis, the m-ZrO_2 phase disappears when the CaO content reaches 15 mol%,

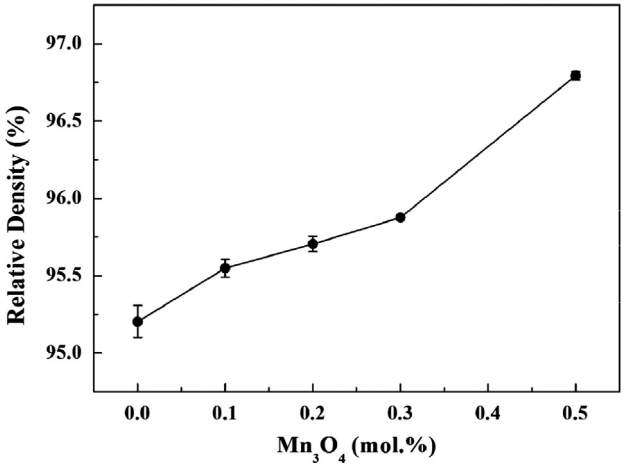

Fig. 4. Relative density as a function of Mn_3O_4 addition for 125CSZ ceramics sintered at 1500 °C for 3 h.

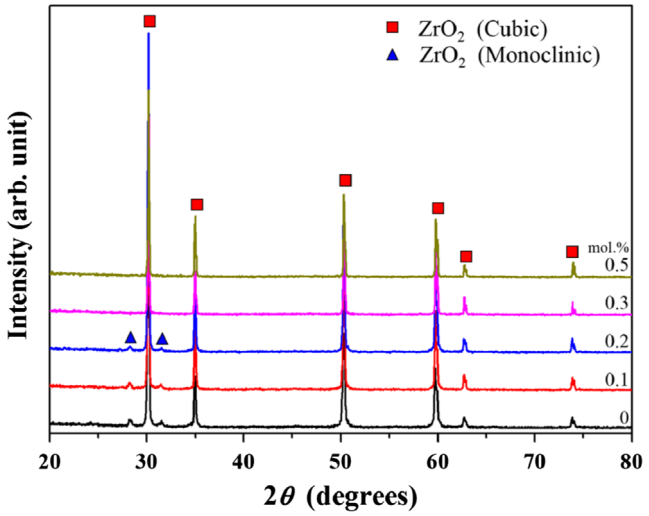

Fig. 5. XRD spectra of the 125CSZ ceramics with different amounts of Mn_3O_4 addition sintered at 1500 °C for 3 h.

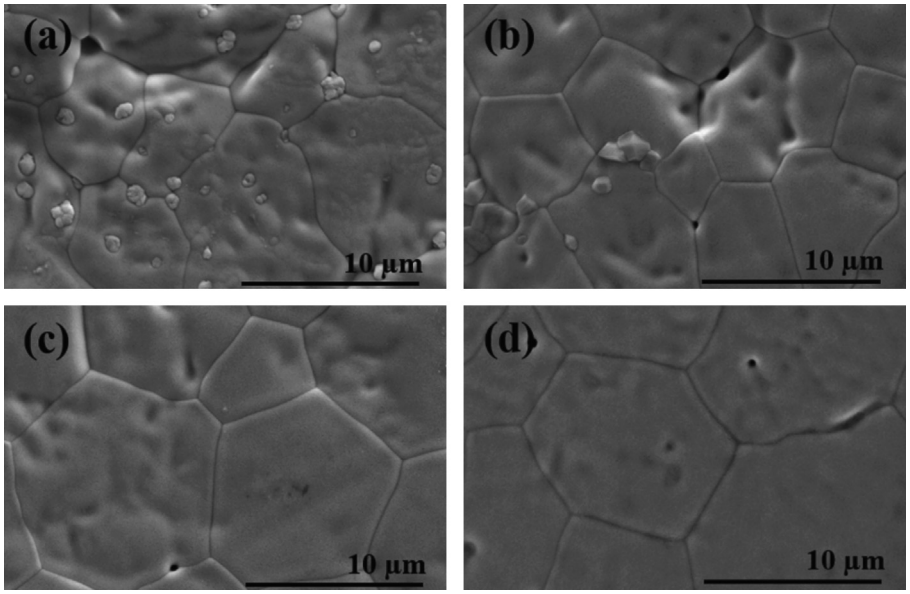

Fig. 6. SEM micrographs of the 125CSZ ceramics with (a) 0.1, (b) 0.2, (c) 0.3, (d) 0.5 mol% Mn_3O_4 addition sintered at 1500 °C for 3 h.

which shows a consistent tendency. Therefore, the small and large grains may be m-ZrO_2 and c-ZrO_2, respectively.

The effects of Mn_3O_4 doping on the relative densities, microstructural characteristics, and phase evolution of the 125CSZ ceramic were evaluated. The relative density of 125CSZ ceramics sintered at 1500 °C for 3 h were measured as a function of Mn_3O_4 addition and are plotted in Fig. 4. The relative density increased to 96.8% with increasing Mn_3O_4 content up to 0.5 mol%. This result is similar to that of Sakka et al. [16], who reported enhancement of densification in 3 mol % YSZ ceramics with 0.1 mol% Mn_3O_4. Addition of Mn_3O_4 thus promotes the diffusion rate of Zr^{4+} ions because the densification rate of ZrO_2 ceramics depends on the diffusion rate of Zr^{4+} [17,18].

The crystalline phases of the five Mn_3O_4-containing samples were determined by XRD. Fig. 5 shows the XRD spectra of 125CSZ ceramics with 0, 0.1, 0.2, 0.3, and 0.5 mol% Mn_3O_4 and sintered at 1500 °C for 3 h. A change in crystalline phase was observed with increasing Mn_3O_4 content. Undoped 125CSZ ceramic has two phases: c-ZrO_2 and m-ZrO_2. The intensity of the peaks of monoclinic phases decreased as the Mn_3O_4 content increased to 0.2 mol% and then disappeared when the Mn_3O_4 content reached 0.3 mol%. These results indicate that addition of Mn_3O_4 is an effective approach for stabilizing ZrO_2 in its cubic phase at room temperature. The oxidation state of Mn in solid solutions with ZrO_2 exists as a mixture of Mn^{2+} and Mn^{3+} when Mn-doped ZrO_2 ceramics are sintered in air [11]. Two double-ionized oxygen vacancies are formed simultaneously when Mn ions are substituted into the Zr site, i.e.:

$$Mn_3O_4 \overset{ZrO_2}{\Longrightarrow} 2Mn'_{Zr} + Mn''_{Zr} + 2V_O^{\bullet\bullet} + 4O_O^X \quad (1)$$

where Mn_{Zr}' is the Mn^{3+} ion on a zirconium lattice site, Mn_{Zr}'' the Mn^{2+} ion on a zirconium lattice site, $V_O^{\bullet\bullet}$ the double positively charged oxygen vacancy, and O_O^X the oxygen neutral atom on an oxygen lattice site. The reaction shows that increasing the Mn content in CSZ results in an increase in concentration of oxide vacancies. Oxygen vacancies have been reported to exert important effects that can promote retention of the cubic phase at room temperature. Cubic to monoclinic phase transformation is driven by a decrease in oxygen vacancies and modification of the valence state of Mn ions [19].

Fig. 6 presents SEM micrographs showing different surface morphologies of 125CSZ ceramics with 0.1, 0.2, 0.3, and 0.5 mol% Mn_3O_4 and sintered at 1500 °C for 3 h. 125CSZ with lower Mn_3O_4 contents showed large grains accompanied by small crystals [Fig. 6(a) and (b)]. With further increases in Mn_3O_4 content, typical equiaxial grains were obtained and good particle packing was achieved [Fig. 6(c) and (d)]. Grain growth rapidly increased with increasing amount of Mn_3O_4 added, as shown in Fig. 7. Thus, Mn_3O_4 can affect the mobility of the grain boundary of ZrO_2 phases.

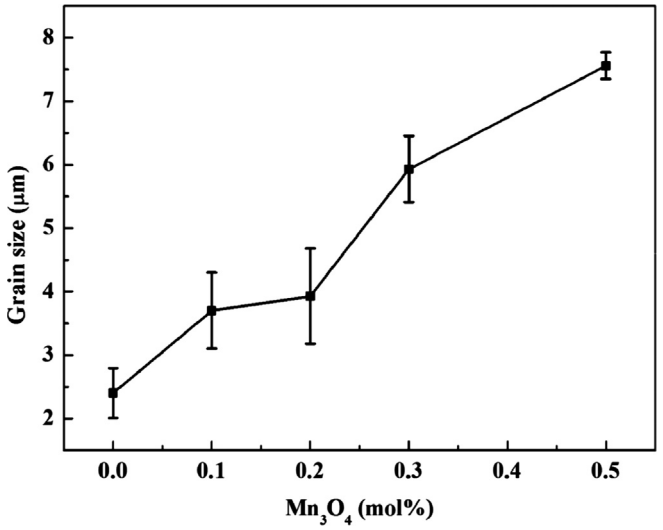

Fig. 7. Average grain size as a function of Mn_3O_4 addition for 125CSZ ceramics sintered at 1500 °C for 3 h.

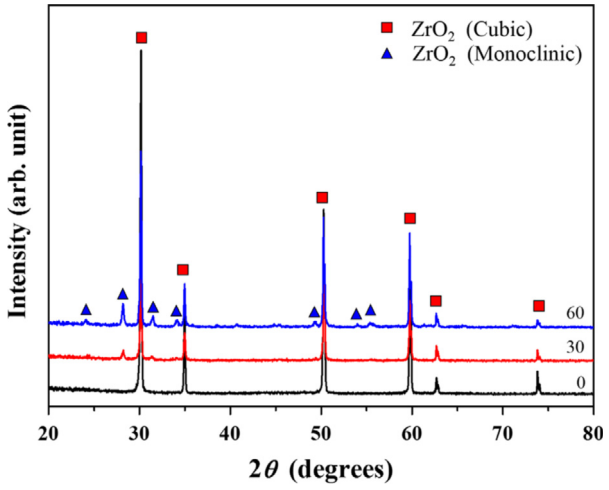

Fig. 8. XRD spectra of the 15CSZ ceramics sintered at 1500 °C for 3 h and subsequently annealed at 1300 °C for 0, 30 and 60 cycles.

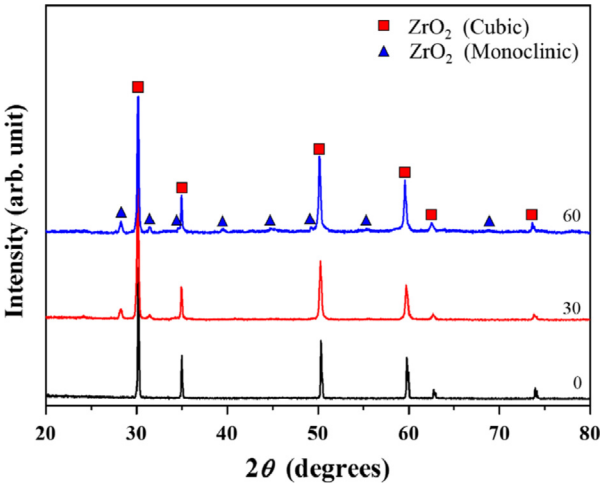

Fig. 9. XRD spectra of the Mn125CSZ ceramics sintered at 1500 °C for 3 h and subsequently annealed at 1300 °C for 0, 30 and 60 cycles.

Table 1
The volume fraction of the m-ZrO_2 for undoped 15CSZ and Mn125CSZ ceramics with annealing treatment for 30 and 60 cycles.

Sample	Thermal aging cycle	Volume fraction of m-ZrO_2 (%)
15CSZ	30	8.1
	60	12.2
Mn125CSZ	30	6.9
	60	9.7

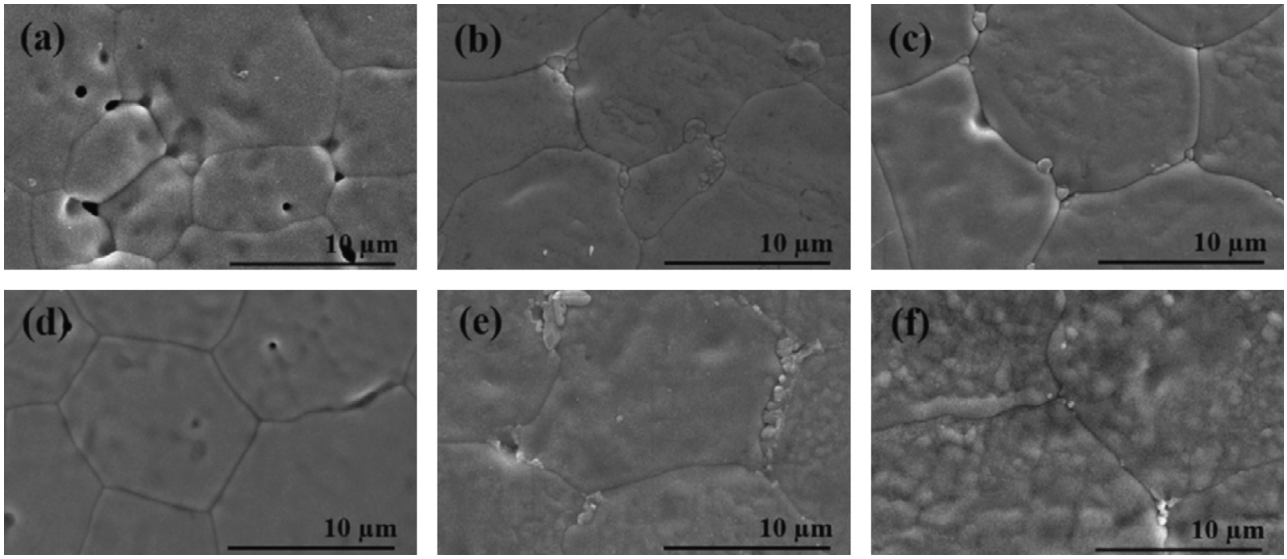

Fig. 10. SEM micrographs of (a–c) 15CSZ and (d–f) Mn125CSZ sintered at 1500 °C for 3 h and subsequently annealed at 1300 °C for 0, 30, and 60 cycles, respectively.

3.2. Phase stability of CSZ and Mn_3O_4-doped CSZ

A thermal aging test was conducted to understand the phase stability of undoped 15CSZ and 0.5 mol% Mn125CSZ ceramics annealed in a reducing atmosphere. The sintered specimens were annealed at 1300 °C for 2 h, and then cooled to room temperature in a reducing atmosphere, which is defined as one cycle for the thermal aging test. Fig. 8 shows the XRD spectra of the undoped 15CSZ ceramics heat treated for 0, 30, and 60 cycles. The as-sintered specimens showed a single cubic structure. The peak of the m-ZrO_2 phase appeared after 30 thermal aging cycles, which means that c-ZrO_2 and m-ZrO_2 coexist in 15CSZ ceramics after heat treatment. In the thermal aging test of 60 cycles, the intensity of the m-ZrO_2 peak also increased compared with that of the c-ZrO_2 peak, which indicates that more m-ZrO_2 precipitates from the c-ZrO_2 matrix. Similar results were observed in the case of the Mn_3O_4-doped CSZ ceramics. Fig. 9 shows the XRD spectra of the Mn125CSZ ceramics sintered at 1500 °C for 3 h and subsequently annealed at 1300 °C for 0, 30, or 60 cycles in a reducing atmosphere. A single crystalline phase of c-ZrO_2 was present in the as-sintered specimens, and two phases (c-ZrO_2 and m-ZrO_2) were observed in the samples annealed for 30 and 60 cycles. The phase evolution of CSZ ceramics during sintering and subsequent lower-temperature annealing can be clearly understood by referencing their phase diagram [9]. At 1300 °C, ZrO_2 with 15 mol% CaO exhibits two phases (tetragonal+cubic phases) in the two-component system [9]. Ciacchi et al. [20] observed that annealing causes formation of tetragonal precipitates.

The XRD spectra in Figs. 8 and 9 show that the m-ZrO_2 phase appears as a secondary phase in undoped 15CSZ and Mn125CSZ annealed for 30 and 60 cycles. The volume fraction of m-ZrO_2 is presented in Table 1. As heat treatment progressed, the amount of m-ZrO_2 observed increased. After heat treatment, Mn125CSZ showed less m-ZrO_2 formation than 15CSZ, which indicates that addition of a small amount of Mn_3O_4 to CSZ produces higher temperature phase stability than pure CSZ.

Minor precipitates of the Mn125CSZ specimens were obtained after thermal aging in a reducing atmosphere. Kawada et al. [10] suggested that Mn ions in stabilized ZrO_2 have a valence of 2+ at oxygen partial pressures lower than 10^{-10} Pa. Mn ions are reduced to lower valence states according to [21]:

$$2Mn_{Mn}^{X} + O_{O}^{X} = \frac{1}{2}O_2 + V_{O}^{\bullet\bullet} + 2Mn_{Mn}^{'} \quad (2)$$

where Mn_{Mn}^{X} is the Mn^{3+} ion on a manganese lattice site, $Mn_{Mn}^{'}$ the Mn^{2+} ion on a manganese lattice site, $V_{O}^{\bullet\bullet}$ the double

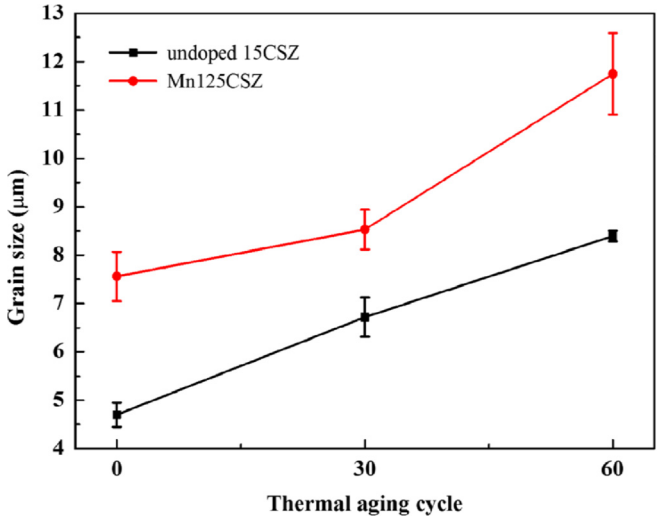

Fig. 11. Average grain size as a function of thermal aging cycle for 15CSZ and Mn125CSZ ceramics.

positively charged oxygen vacancy, and O_O^X the oxygen neutral atom on an oxygen lattice site. Extra oxygen vacancies are generated when Mn^{2+} ions are substituted into Zr^{4+} sites during heat treatment, resulting in the stable presence of the c-ZrO_2 phase at room temperature.

Although substitution of Ca^{2+} and Mn^{2+} for Zr^{4+} in the ZrO_2 lattice could generate oxygen vacancies, the contribution of Mn^{2+} to the stabilized ZrO_2 is higher than that of Ca^{2+}, which could be ascribed to the different ionic radii of the cations (Ca^{2+} = 0.112 nm, Mn^{2+} = 0.096 nm) [7,22]. Barker et al. [23] suggested that the amount of added stabilizer could be reduced in the case of fully stabilized ZrO_2 when the radius of the cationic stabilizer is close to that of Zr^{4+} (0.084 nm). Jones et al. [24] and Leoni et al. [25] investigated changes in the formation of monoclinic ZrO_2 with respect to the stabilizer and reported that scandia-YSZ shows better phase stability than conventional YSZ; here, the ionic radii of Y^{3+} and Sc^{3+} are 0.102 nm and 0.087 nm, respectively.

SEM micrographs of 15CSZ and Mn125CSZ ceramics subjected to annealing treatment for 0, 30, and 60 cycles are presented in Fig. 10. Fig. 10(a) and (d) shows the morphology of undoped 15CSZ and Mn125CSZ ceramics without annealing treatment, respectively. XRD results indicate that typical equiaxial grains of c-ZrO_2 were obtained. Grain boundaries were clearly observed, and the grain sizes of 15CSZ and the Mn125CSZ were about 4.7 and 7.6 μm, respectively. Fig. 10 (b), (c), (e), and (f) shows that the fine grains may represent the m-ZrO_2 phase in the c-ZrO_2 matrix, similar to Fig. 3(e). The grain sizes of 15CSZ and Mn125CSZ annealed at 1300 °C for 60 cycles were approximately 8.4 and 11.8 μm, respectively. The grain size data of 15CSZ and Mn125CSZ after annealing for 0, 30, and 60 cycles are shown in Fig. 11.

4. Conclusions

In this study, the effects of doping with Mn_3O_4 and annealing under a reducing atmosphere on the phase evolution, microstructure, and phase stability of CSZ ceramics were investigated. A single c-ZrO_2 phase was successfully prepared by the solid-state reaction of 0.3 mol% Mn_3O_4-doped 125CSZ ceramic at a sintering temperature of 1500 °C. The m-ZrO_2 phase was precipitated within the c-ZrO_2 matrix when undoped 15CSZ and Mn125CSZ as-sintered ceramics were annealed at 1300 °C for 30 cycles in a reducing atmosphere. These results suggest that the stability of the c-ZrO_2 phase of Mn_3O_4-CaO-stabilized ZrO_2 is better than that of commercial 15CSZ at 1300 °C. Mn_3O_4-doped 125CSZ showed significant grain growth, which is attributed to oxygen vacancies that enhance the atomic mobility of the grain boundaries.

Acknowledgment

The authors would like to acknowledge the financial support of this research by the National Science Council of Taiwan under contract no. NSC-100-2221-E-005-034-MY3.

References

[1] W. Pyda, A. Pyda, Effect of sintering environment on the structure of calcia-stabilised TiO_2-added zirconia solid solutions, Journal of the European Ceramic Society 27 (2–3) (2007) 769–773.
[2] A.K. Bhattacharya, P. Reinhard, W. Steurer, V. Shklover, Calcia-doped yttria-stabilized zirconia for thermal barrier coatings: synthesis and characterization, Journal of Materials Science 46 (17) (2011) 5709–5714.
[3] N. Moskala, W. Pyda, Thermal stability of tungsten carbide in 7 mol% calcia-zirconia solid solution matrix heat treated in argon, Journal of the European Ceramic Society 26 (16) (2006) 3845–3851.
[4] R.I. Merino, J.I. Pena, M.A. Laguna-Bercero, A. Larrea, V.M. Orera, Directionally solidified calcia stabilised zirconia-nickel oxide plates in anode supported solid oxide fuel cells, Journal of the European Ceramic Society 24 (6) (2004) 1349–1353.
[5] R. Muccillo, R.C. Buissa Netto, Muccillo ENS. Synthesis and characterization of calcia fully stabilized zirconia solid electrolytes, Materials Letters 49 (3-4) (2001) 197–201.
[6] S. Nath, N. Sinha, B. Basu, Microstructure, mechanical and tribological properties of microwave sintered calcia-doped zirconia for biomedical applications, Ceramics International 34 (6) (2008) 1509–1520.
[7] D.J. Green, R.H.J. Hannink, M.V. Swain, Transformation Toughening of Ceramics, CRC Press, Inc., Florida, 1989.
[8] P. Duwez, F. Odell, F.H.J.R. Brown, Stabilization of zirconia with calcia and magnesia, Journal of the American Ceramic Society 35 (5) (1952) 107–113.
[9] V.S. Stubican, S.P. Ray, Phase equilibria and ordering in the system ZrO_2-CaO, Journal of the American Ceramic Society 60 (11-12) (1977) 534–537.
[10] T. Kawada, N. Sakai, H. Yokokawa, M. Dokiya, Electrical properties of transition-metal-doped YSZ, Solid State Ionics 53-56 (1992) 418–425.
[11] C.C. Appel, G.A. Botton, A. Horsewell, W.M. Stobbs, Chemical and structural changes in manganese-doped yttria-stabilized zirconia studied by electron energy loss spectroscopy combined with electron diffraction, Journal of the American Ceramic Society 82 (2) (1999) 429–435.
[12] H. Yokokawa, N. Sakai, T. Kawada, M. Dokiya, Thermodynamic analysis of solubilities and valence state of transition metal ions in yttria stabilized zirconia, International Society for Solid State Ionics 2 (1991) 7–8.
[13] H.G. Scott, Phase relationships in the zirconia-yttria system, Journal of Materials Science 10 (9) (1975) 1527–1535.
[14] K.C. Radford, R.J. Bratton, Zirconia electrolyte cells, Journal of Materials Science 14 (1) (1979) 59–65.

[15] R.P. Ingel, D. Lewis III, Lattice parameters and density for Y_2O_3-stabilized ZrO_2, Journal of the American Ceramic Society 69 (4) (1986) 325–332.
[16] Y. Sakka, T. Ishii, T.S. Suzuki, K. Morita, K. Hiraga, Fabrication of high-strain rate superplastic yttria-doped zirconia polycrystals by adding manganese and aluminum oxides, Journal of the European Ceramic Society 24 (2) (2004) 449–453.
[17] K. Matsui, N. Ohmichi, M. Ohgai, H. Yoshida, Y. Ikuhara, Effect of alumina-doping on grain boundary segregation-induced phase transformation in yttria-stabilized tetragonal zirconia polycrystal, Journal of Materials Research 21 (9) (2006) 278–289.
[18] M. Hartmanova, F.W. Poulsen, F. Hanic, K. Putyera, D. Tunega, A.A. Urusovskaya, T.V. Oreshnikova, Influence of copper- and iron-doping on cubic yttria-stabilized zirconia, Journal of Materials Science 29 (8) (1994) 2152–2158.
[19] L. Gao, L. Zhou, C.S. Li, J.Q. Feng, Y.F. Lu, Structure evolution of manganese stabilized zirconia, Journal of Optoelectronics and Advanced Materials 6 (1-2) (2012) 178–182.
[20] F.T. Ciacchi, S.P.S. Badwal, J. Drennan, The system Y_2O_3-Sc_2O_3-ZrO_2: Phase characterisation by XRD, TEM and optical microscopy, Journal of the European Ceramic Society 7 (3) (1991) 185–195.
[21] M.K. Mahapatra, S. Bhowmick, N. Li, P. Singh, Role of oxygen pressure on the stability of lanthanum strontium manganite-yttria stabilized zirconia composite, Journal of the European Ceramic Society 32 (10) (2012) 2341–2349.
[22] R.D. Shannon, Revised effective ionic radii and systematic studies of interatomic distances in halides and chalcogenides, Acta Crystallographica A32 (1976) 751–767.
[23] W.W. Barker, L.S. Williams, Some limitations of cubic stabilization of zirconia, Journal of the Australian Ceramic Society 4 (1) (1968) 1–5.
[24] R.L. Jones, R.F. Reidy, Mess D. Scandia, yttria-stabilized zirconia for thermal barrier coatings, Surface and Coatings Technology 82 (1-2) (1996) 70–76.
[25] M. Leoni, R.L. Jones, P. Scardi, Phase stability of scandia-yttria-stabilized zirconia TBCs, Surface and Coatings Technology 108-109 (1998) 107–113.